LOW FREQUENCY STRUCTURAL AND ACOUSTIC RESPONSES OF A SUBMARINE HULL

Mauro Caresta, Nicole Kessissoglou
School of Mechanical and Manufacturing Engineering
University of New South Wales (UNSW)
Sydney, NSW 2052, Australia

Yan Tso
Maritime Platforms Division
Defence Science and Technology Organisation
Fishermans Bend VIC 3207, Australia

ABSTRACT: A model to describe the low frequency dynamic and acoustic responses of a submarine hull subject to a harmonic propeller shaft excitation is presented. The submarine is modelled as a fluid-loaded, ring stiffened cylindrical shell with internal bulkheads and end caps. The stiffeners are introduced using a smeared approach. The bulkheads are modelled as circular plates and the end closures as truncated conical shells. The propeller introduces a harmonic axial force that is transmitted to the hull through the shaft and results in excitation of the accordion modes only if the force is symmetrically distributed to the hull. Structural and acoustic responses for the axisymmetric breathing modes are presented in terms of frequency response functions of the axial and radial displacements and directivity patterns for the radiated sound pressure.

1. INTRODUCTION

Vibration modes of a submerged hull are excited from the transmission of fluctuating forces through the shaft and thrust bearings due to the propeller rotation. These low frequency vibration modes of the hull can result in a high level of radiated noise. A hull can be idealised as a finite cylinder submerged in a fluid. The dynamic responses of cylindrical shells has received much research attention, ranging from the free vibrational characteristics of isotropic cylindrical shells subject to various boundary conditions [1, 2], to the effect of structural discontinuities such as stiffeners, a junction or changes in diameter on the wave propagation [3-5]. Thin cylindrical shells are often periodically stiffened in order to both increase stiffness and strength and reduce weight. Cylinders may be stiffened by circumferential rings, longitudinal stringers or both, in which the stiffeners are modelled as discrete elements [6-11] or their properties are averaged over the surface of the shell [12]. For submerged vessels, the effect of fluid loading on the structural and acoustic responses of cylindrical shells have been investigated [13-15].

In previous work by the authors [16], the submerged body was modelled as a ring-stiffened cylindrical shell with finite end closures and separated by bulkheads into a number of compartments. Excitation from the propeller/propulsion is idealised as an axial excitation acting at one end of the hull. This gives rise to excitation of the hull axisymmetric breathing modes associated with the zeroth circumferential mode number (n=0). This paper expands on this previous work to include the effect of end closures which are modelled as truncated conical shells. The forced response of the structure is calculated by solving the cylindrical shell displacements in the form of a wave solution and the conical shell in terms of a power series. An analytical expression for the radiated sound pressure from the structure is presented and accounts for the contributions from both the cylindrical hull and the end caps. Once the radial displacement of the structure is determined, the sound radiation in the far field is evaluated by modelling the submarine as a slender axisymmetric body for which the closed form solution of the Helmholtz equation is possible. The radiating surface is considered continuous. The scattering from the curvature discontinuity at the junction between the cylindrical and conical shells is neglected as well as the scattering at the external plates closing the conical shells. At low frequencies (<100 Hz), these effects are considered negligible.

2. DYNAMIC MODEL OF THE SUBMARINE HULL

Cylindrical shell

The submarine is modelled as a fluid loaded cylindrical shell with internal bulkheads and ring stiffeners. The hull is closed by means of end plates and truncated conical shells. The truncated cones are also closed at each end by circular plates. The model is illustrated in Figure 1. The main part of the submarine consists of a finite ring stiffened cylindrical shell closed at each end by two circular plates. The hull is partitioned into three parts by two equally spaced bulkheads. The ring stiffeners are modelled using smeared theory [12].

In Figure 2, u, v and w are the orthogonal components of displacement in the x, θ and z directions, respectively. a is the mean radius of the cylindrical shell and h is the shell thickness.

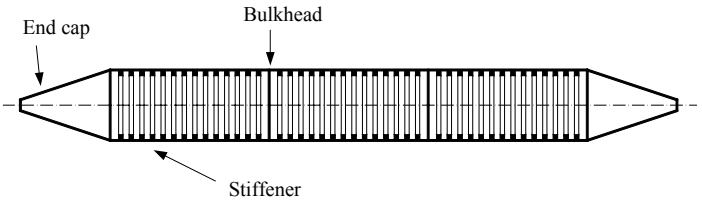

Figure 1. Schematic diagram of the submarine.

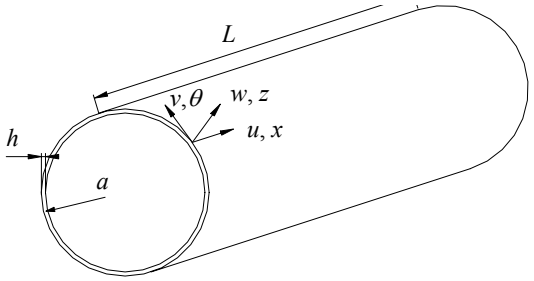

Figure 2. Coordinate system and displacements for a thin walled cylindrical shell.

Variation to the differential equations of motion for thin cylindrical shells have been summarised by Leissa [1]. Flügge equations of motion were used and can be written in terms of a differential operator L_{ij} by [17]

$$L_{11}u + L_{12}v + L_{13}w = 0 \tag{1}$$

$$L_{21}u + L_{22}v + L_{23}w = 0 \tag{2}$$

$$L_{31}u + L_{32}v + L_{33}w - \frac{p}{\rho h c_L^2} = 0 \tag{3}$$

The elements of the matrix differential operator L_{ij} used in Eqs. (1) to (3) according to the Flügge theory can be found in the Appendix. $c_L = [E/\rho(1-\upsilon^2)]^{1/2}$ is the longitudinal wave speed. E, ρ and υ are respectively the Young's modulus, density and Poisson's ratio of the cylinder. The external pressure loading p due to the fluid acting normally to the surface of the cylindrical shell can be approximated using an infinite model and expressed in terms of a fluid loading parameter F_L by [18]

$$p = \frac{\rho h c_L^2}{a^2} F_L w \tag{4}$$

$$F_L = -\Omega^2 \frac{a}{h}\frac{\rho_f}{\rho}\frac{H_n(k_{nr}a)}{H_n'(k_{nr}a)} \tag{5}$$

where $\Omega = \omega a/c_L$ is the non dimensional ring frequency, ρ_f is the density of the fluid. H_n is the Hankel function of order n and H'_n is its derivative with respect to the argument. k_{nr} is the radial wavenumber [18]. The general solutions to the equations of motion can be written as

$$w = \sum_{n=0}^{\infty}\sum_{i=1}^{8} W_{n,i} e^{jk_{n,i}x}\cos(n\theta)e^{-j\omega t} \tag{6}$$

$$u = \sum_{n=0}^{\infty}\sum_{i=1}^{8} C_{n,i}W_{n,i} e^{jk_{n,i}x}\cos(n\theta)e^{-j\omega t} \tag{7}$$

$$v = \sum_{n=0}^{\infty}\sum_{i=1}^{8} G_{n,i}W_{n,i} e^{jk_{n,i}x}\sin(n\theta)e^{-j\omega t} \tag{8}$$

where $C_{n,i}=U_{n,i}/W_{n,i}$ and $G_{n,i}=V_{n,i}/W_{n,i}$. $k_{n,i}$ is the axial wavenumber and n is the circumferential mode number.

End plates and bulkheads

The end plates and bulkheads were modelled as thin circular plates in bending and in-plane motion. The axial w_p, radial u_p and circumferential v_p plate displacements are shown in Figure 3. h_p is the plate thickness.

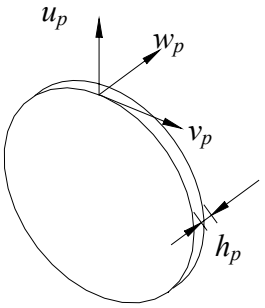

Figure 3. Displacements for a thin circular plate.

Displacements for the end plates and bulkheads can be written as [3]

$$w_p = \sum_{n=0}^{\infty}\left(A_{n,1}J_n(k_{pB}a) + A_{n,2}I_n(k_{pB}a)\right)\cos(n\theta)e^{-j\omega t} \tag{9}$$

$$u_p = \sum_{n=0}^{\infty}\left(B_{n,1}\frac{\partial J_n(k_{pL}a)}{\partial a} + \frac{nB_{n,2}J_n(k_{pT}a)}{a}\right)\cos(n\theta)e^{-j\omega t} \tag{10}$$

$$u_p = \sum_{n=0}^{\infty}\left(B_{n,1}\frac{\partial J_n(k_{pL}a)}{\partial a} + \frac{nB_{n,2}J_n(k_{pT}a)}{a}\right)\cos(n\theta)e^{-j\omega t} \tag{11}$$

where k_{pB} is the plate bending wavenumber and k_{pT}, k_{pL} are the wavenumbers for in-plane waves in the plate [3]. J_n, I_n are respectively Bessel functions and modified Bessel functions of the first kind. The coefficients $A_{n,j}$ and $B_{n,j}$ (j=1,2) are determined from the continuity equations at the cylinder/plate junctions.

Conical shell

Dynamic modelling of the conical shells can be found in [19]. The displacement of the conical shell was described using a power series solution following the procedure presented by Tong [20]. The displacements and coordinate system for the conical shell are shown in Figure 4, where u_c and v_c are respectively the displacements of the shell's middle surface along the x_c and θ_c directions. w_c is the displacement normal to the surface along the z_c direction.

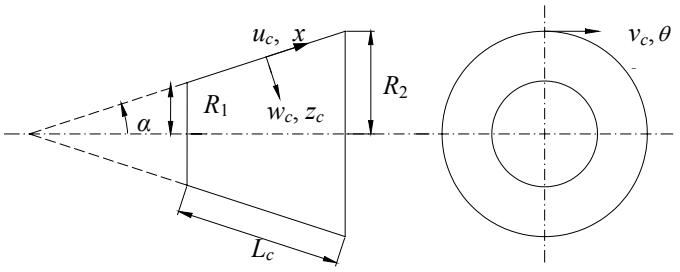

Figure 4. Coordinate system for a thin truncated conical shell.

External fluid loading on the conical shell was taken into account using a local cylindrical approximation which is described in what follows. The conical shell is divided in several narrow segments, as shown in Figure 5. The segments are narrow enough to be considered as locally cylindrical in order to account for the fluid loading; that is, the fluid loading on the conical strip is considered the same acting on an equivalent cylindrical shell with the same width and radius R_i. This approximation is only applicable to the calculation of the fluid loading acting on a shell segment. To solve for conical shell displacements, the equations of motion and corresponding general solutions for a conical shell were used. This method of accounting for the fluid loading acting on a conical shell using a local cylindrical approximation is shown to be reliable at low frequencies [19].

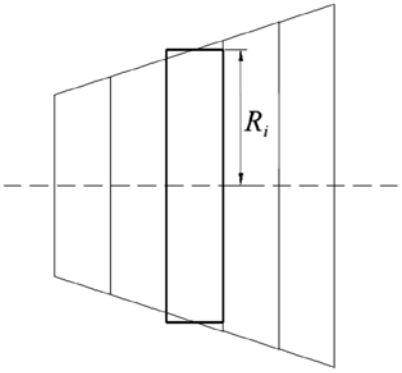

Figure 5. Local approximation of the conical shell.

Propeller shaft excitation

The propeller force is transmitted to the edge of the cylindrical section of the hull. The transmitted force can be modelled as an axisymmetric distributed load given by $F=F_o/2\pi a$ as shown in Figure 6. The distributed load excites only the n=0 breathing modes.

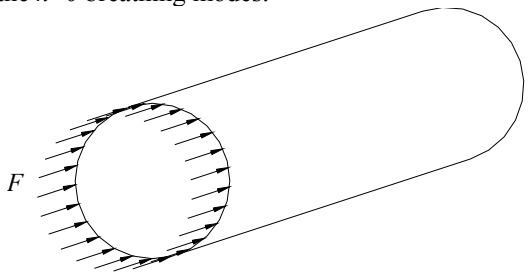

Figure 6. Distributed force excitation of the hull.

The dynamic response of the submarine for each value of the circumferential mode number n is expressed in terms of $A_{n,j}$ and $B_{n,j}$ (j=1,2 for each circular plate) and $W_{n.i}$ (i=1:8 for each section of the hull). The entire submarine is free-free. At the cylinder/plate junctions, continuity of displacements and equilibrium of forces/moments have to be satisfied. The whole structure consists of three cylindrical shell segments, six circular plates and two truncated conical shells. The boundary and continuity equations can be arranged in matrix form **BX**=**F**, where **X** is the vector of unknown coefficients and **F** is the vector containing the external fluctuating forces from the propeller. Once the unknown coefficients have been determined the radial displacement of the hull can be obtained.

3. FAR FIELD SOUND PRESSURE

After the radial displacement of the structure has been determined, the far field sound pressure P can be evaluated following the procedure presented by Skelton and James [21]. The submarine structure can be viewed as a slender body of revolution. The cylindrical coordinate systems are (r, θ_r, z_r) for the exterior body and (r_0, θ_0, z_0) on the surface of the structure, as shown in Figure 7.

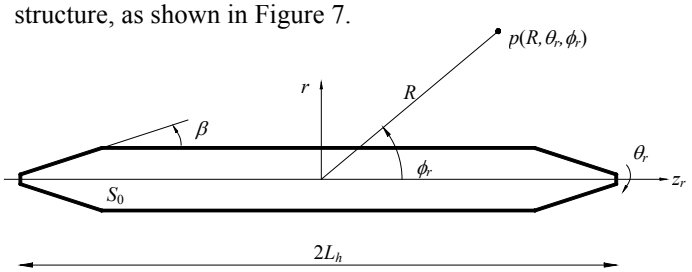

Figure 7. Coordinate system for the far field point.

The angle β is defined by $\tan\beta=\partial a_r(z_r)/\partial z_r$ where a_r is the radius of the structure at location z_r and $2L_h$ is the total length of the structure. The displacement normal to the surface, calculated solving the matrix **BX**=**F**, can be written as

$$W_N(r_0,\theta_0,z_0)=\sum_{n=0}^{\infty}W_N(r_0,z_0)\cos(n\theta_0) \tag{12}$$

Considering a local approximation for the pressure near the surface of the body, the sound pressure in the far field can be calculated and expressed in polar coordinates by

$$P(R,\phi_r,\theta_r)=\frac{\omega\rho_f c_f e^{jk_f R}}{2R}\sum_{n=0}^{\infty}-j^n X_n(k_f\cos\phi_r)\cos(n\theta_r) \tag{13}$$

where

$$X_n(k_f\cos\phi_r)=\int_{-L_h}^{L_h}\frac{I(\gamma a_r)W_n(a_r,z_0)a_r(z_0)}{\omega\rho_f c_f\cos\beta}e^{-jk_f\cos\phi_r z_0}dz_0 \tag{14}$$

$$I(\gamma a_r)=-k_f J_n(\gamma a_r)$$
$$+\frac{H_n(k_f a_r\cos\beta)(\gamma\cos\beta J_n'(\gamma a_r)+j\alpha\sin\beta J_n(\gamma a_r))}{\cos^2\beta H_n'(k_f a_r\cos\beta)+j\sin^2\beta H_n(k_f a_r\cos\beta)} \tag{15}$$

k_f is the acoustic wavenumber and c_f is the speed of sound in the medium. The integral in Eq. (14) can be calculated by considering separately the contribution of each section of the submarine corresponding to the conical and cylindrical shells. In this analysis, the surface is considered continuous.

Figure 6 Distributed force excitation of the hull.

Scattering from the curvature discontinuity at the junction between the cylindrical and conical shells and between the cones and the external plates are neglected.

4. RESULTS

Numerical results are presented for a ring-stiffened steel cylinder of radius a=3.25m, hull plate thickness h=0.04m, length L=45m and with two evenly spaced bulkheads of thickness h_p=0.04m. The end plates at each end of the cylinder are also of thickness h_p=0.04m. The conical end enclosures are of dimensions h_c=0.014m, R_1=0.50m, R_2=3.25m, $\alpha=\pi/10$rad. The material properties of steel are density ρ=7800kgm^{-3}, Young's modulus E=21x10^{11}Nm^{-2} and Poisson's ratio υ=0.3. The stiffeners have a rectangular cross-sectional area of 0.08m x 0.15m and are evenly spaced by 0.5m. The cylinder was submerged in water (ρ_f=1000kgm^{-3}). The onboard equipment and ballast tanks are taken into account considering a distributed mass on the shell of m_{eq}=1500kgm^{-2}. Internal structural damping was included in the analysis using a structural loss factor of 0.02. The submarine was excited with an axial force of unity amplitude F_o=1N applied to one end of the finite cylindrical shell. Only the natural frequencies of the breathing modes defined by the n=0 circumferential mode were excited, resulting in axisymmetric motion of the hull. The structural results are presented in terms of the frequency response function of the axial and radial displacements at the ends of the cylindrical section. The acoustic results are presented in terms of the maximum sound pressure evaluated in the far field at θ_r=0 and R=1000m.

Structural response

Figures 8 and 9 present the frequency response functions (FRFs) of the axial and radial displacements at each end of the cylindrical shell corresponding to x=0 and L. In Figure 8, the main peaks occurring at 22.7, 45.4 and 67.9 Hz are the first three resonant frequencies of the submarine for the axisymmetric case (n=0 breathing modes). The small peaks occurring at approximately 9 and 36 Hz are due to the bulkheads. The bulkhead resonances are more evident in Figure 9 which shows the radial displacement at each end of the cylindrical shell. As the axisymmetric modes are mainly axial in nature, the radial responses at the bulkhead natural frequencies are comparable with the responses at the resonances of the cylindrical shell.

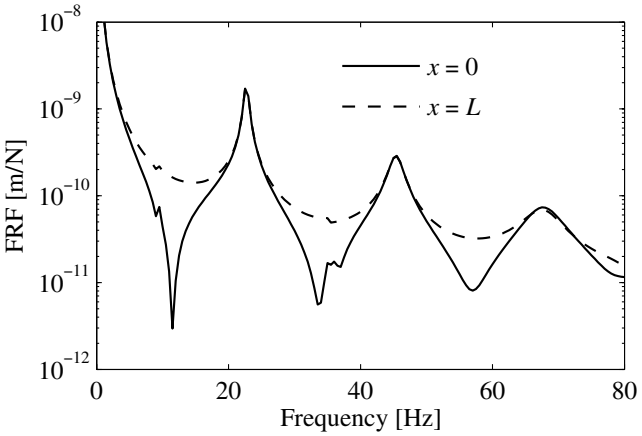

Figure 8. Frequency response of the axial displacement.

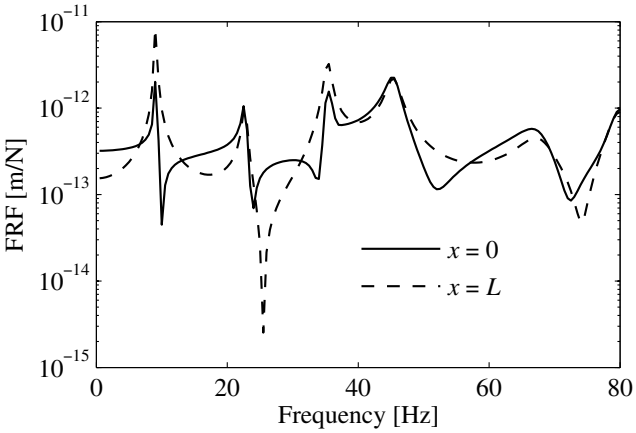

Figure 9. Frequency response of the radial displacement.

The corresponding deformation shapes which are a combination of axial and radial displacements are shown in Figures 10 to 12 for the first three axisymmetric modes, respectively. Different scales are used for the horizontal and vertical axes in order to magnify the radial response. At the first and third resonant frequencies of 22.7 and 67.9 Hz respectively, the ends of the hull are vibrating out of phase with each other. At the second resonant frequency (Figure 11), the ends of the hull are vibrating in phase. The accordion motion of the hull results in large deformation in the axial direction and only a small radial expansion of the central cylindrical hull. The conical shells behave almost rigidly except for a small deformation at the junctions between the cylinder and end plates. The localised effect of the bulkheads on the radial displacement is shown. The effect of the ring stiffeners is not observed as the stiffeners were modelled using orthotropic shell properties. In all figures of the deformation shapes for the first three axisymmetric modes, the contribution of the axial motion and thus the radiation from the end cones result in the maximum values of the radiated sound pressure.

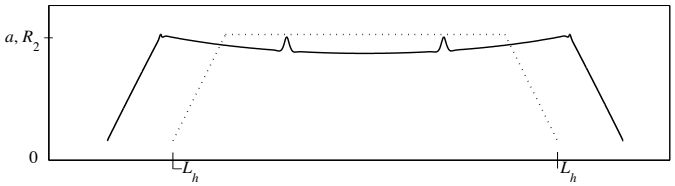

Figure 10. Deformation shape at the first n=0 natural frequency of 22.7 Hz.

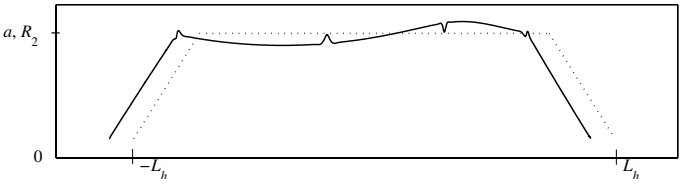

Figure 11. Deformation shape at the second n=0 natural frequency of 45.4 Hz.

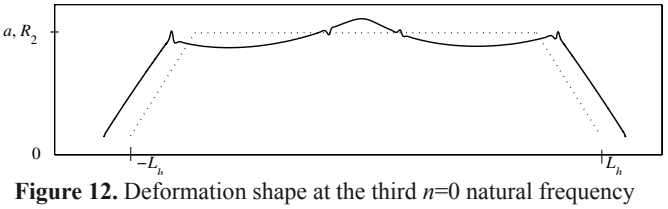

Figure 12. Deformation shape at the third n=0 natural frequency of 67.9 Hz.

Acoustic response

Figure 13 presents the maximum radiated sound pressure, which clearly shows the first three resonant frequencies of the submarine for the axisymmetric case (n=0 breathing modes). Small peaks due to the bulkheads are just visible. The radiation directivity patterns in terms of the angle ϕ_r are shown in Figures 14 to 16 for the first three axisymmetric modes of the submarine, respectively. The contribution from the cylindrical shell to the total radiated pressure is represented by the central lobes in the directivity patterns. The side lobes are due to the contribution from the end cones. As the frequency increases, the radiation directivity increases in complexity. For the first three resonances, there are one, two and three central lobes, respectively. In Figure 14, the directivity pattern shows that the contribution to the total sound pressure from the cones results in large lobes in the axial direction. A partial cancellation due to the pressure radiated by the cylindrical section occurs in the direction normal to the axis of the submarine. At the second natural frequency, the cylindrical section assumes a sinusoidal shape and its directivity pattern is bilobate. Similarly, at the third resonance, the radiated pressure from the central cylindrical shell is trilobite. As expected, the end cones determine the maximum sound pressure since the axisymmetric modes are mainly axial modes with little radial expansion.

5. CONCLUSIONS

An analytical model to study the low frequency structural and acoustic responses of a submerged vessel has been presented. Modelling of the submarine included several influencing factors corresponding to ring stiffeners, bulkheads and fluid-loading. The hull was closed by end plates and truncated conical shells. The truncated cones were solved using a power series solution whereas the hull was solved using a wave solution. The excitation from the propeller shaft results in an axisymmetric force distribution to the cylindrical hull which excites only the accordion modes of zeroth circumferential mode number. Results were presented in terms of frequency responses at each end of the cylindrical hull and of the maximum far field radiated sound pressure. Results were also presented for the deformation shapes and corresponding directivity patterns for the first three axisymmetric modes. Future work will involve extending the analytical model to include the effect of higher order circumferential modes, thus allowing the individual contributions from the higher order circumferential modes on the hull structural and acoustic responses to be observed. Furthermore, the development of an analytical model will allow the implementation of appropriate active control strategies to be investigated.

REFERENCES

[1] A. W. Leissa, *Vibration of shells*, American Institute of Physics, New York, 1993.

[2] L. Cheng and J. Nicolas, "Free vibration analysis of a cylindrical shell-circular plate system with general coupling and various boundary conditions", *Journal of Sound and Vibration*, **155**, 231-247 (1992).

[3] Y. K. Tso and C. H. Hansen, "Wave propagation through cylinder/plate junctions", *Journal of Sound and Vibration*, **186**, 447-461 (1995).

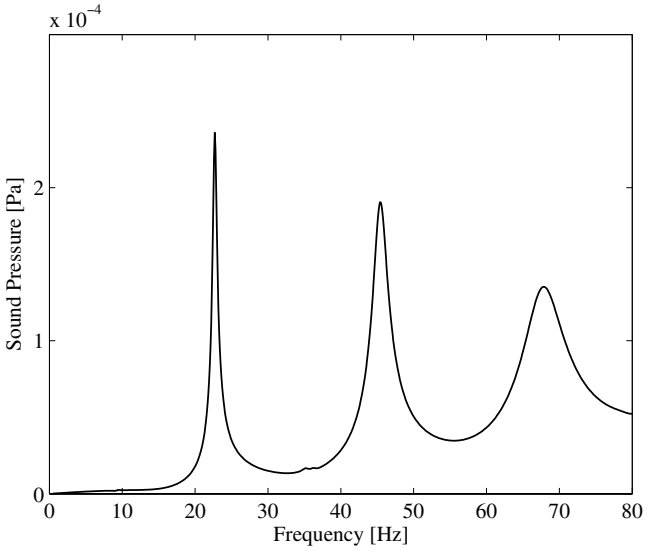

Figure 13. Maximum far field sound pressure, θ_r=0, R=1000 m.

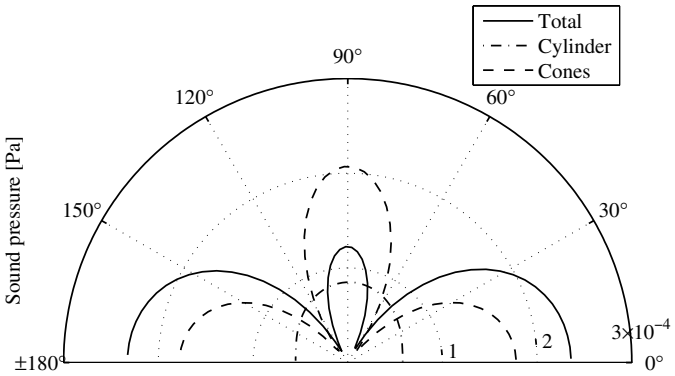

Figure 14. Directivity pattern at the first n=0 natural frequency of 22.7 Hz.

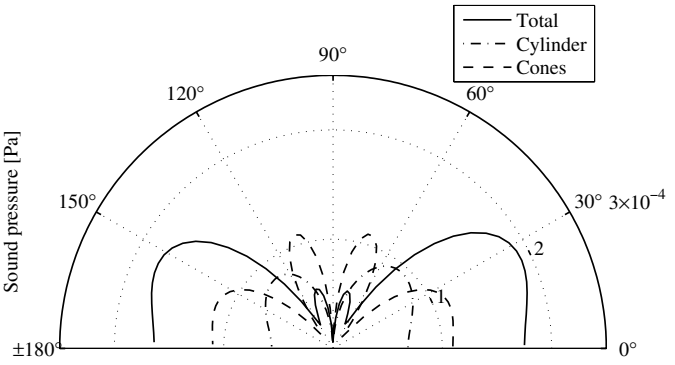

Figure 15. Directivity pattern at the second n=0 natural frequency of 45.4 Hz.

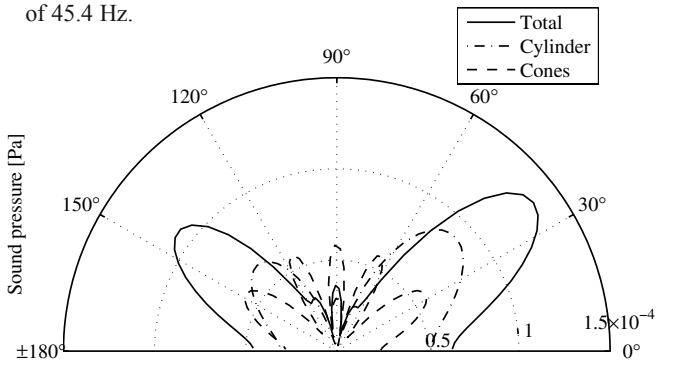

Figure 16. Directivity pattern at the third n=0 natural frequency of 67.9 Hz.

[4] A. Harari, "Wave propagation in cylindrical shells with finite regions of structural discontinuity", *Journal of the Acoustical Society of America*, **62**, 1196-1205 (1977).
[5] C. R. Fuller, "The effects of wall discontinuities on the propagation of flexural waves in cylindrical shells", *Journal of Sound and Vibration*, **75**, 207-228 (1981).
[6] D. M. Egle and J. L. Sewall, "An analysis of free vibration of orthogonally stiffened cylindrical shells with stiffeners treated as discrete elements", *AIAA Journal*, **6**, 518-526(1968).
[7] D. J. Mead and N. S. Bardell, "Free vibration of a thin cylindrical shell with discrete axial stiffeners", *Journal of Sound and Vibration*, **111**, 229-250 (1986).
[8] A. M. J. Al-Najafi and G. B. Warburton, "Free vibration of ring-stiffened cylindrical shells", *Journal of Sound and Vibration*, **13**, 9-25 (1970).
[9] D. E. Beskos and J. B. Oates, "Dynamic analysis of ring-stiffened circular cylindrical shells", *Journal of Sound and Vibration*, **75**, 1-15 (1981).
[10] P. R. Paslay, R. B. Tatge, R. J. Wernick, E. K. Walsh and D. F. Muster, "Vibration characteristics of a submerged ring-stiffened cylindrical shell of finite length", *Journal of the Acoustical Society of America*, **46**, 701-710 (1969).
[11] A. Harari and B. E. Sandman, "Radiation and vibrational properties of submerged stiffened cylindrical shells", *Journal of the Acoustical Society of America*, **88**, 1817-1830 (1990).
[12] W. H. Hoppmann, II, "Some characteristics of the flexural vibrations of orthogonally stiffened cylindrical shells", *Journal of the Acoustical Society of America*, **30**, 77-82 (1958).
[13] G. C. Everstine, "Prediction of low frequency vibrational frequencies of submerged structures", *Journal of Vibration, Acoustics, Stress, and Reliability in Design*, **113**, 187-191 (1991).
[14] J. E. Cole, III, "Vibrations of a framed cylindrical shell submerged in and filled with acoustic fluids: spectral solution", *Computers and Structures*, **65**, 385-393 (1997).
[15] P. R. Stepanishen, "Modal coupling in the vibration of fluid-loaded cylindrical shells", *Journal of the Acoustical Society of America,* **71**, 813-823 (1982).
[16] S. Merz, S. Oberst, P. G. Dylejko, N. J. Kessissoglou, Y.K. Tso and S. Marburg, "Development of coupled FE/BE models to investigate the structural and acoustic responses of a submerged vessel" *Journal of Computational Acoustics*, **15**, 23-47 (2007).
[17] A. Rosen and J. Singer, "Vibrations of axially loaded stiffened cylindrical shells", *Journal of Sound and Vibration*, **34**, 357-378 (1974).
[18] C. R. Fuller, "Radiation of sound from an infinite cylindrical elastic shell excited by an internal monopole source", *Journal of Sound and Vibration*, **109**, 259-275 (1986).
[19] M. Caresta and N. J. Kessissoglou, "Vibration of fluid loaded conical shells", *Journal of the Acoustical Society of America*, **124**, to appear (2008).
[20] L. Tong, "Free vibration of orthotropic conical shells", *International Journal of Engineering Science*, **31**, 719-733 (1993).
[21] E. A. Skelton and J. H. James, *Theoretical acoustics of underwater structures*, Imperial College Press, London, 1997.

APPENDIX: Elements of the Flügge differential operator

The elements of the matrix differential operator L_{ij} used in Eqs. (1) to (3) according to the Flügge theory and modified to take into account the internal ring stiffeners are given by [17]

$$L_{11} = \frac{\partial^2}{\partial x^2} + \frac{q_1(1+\beta^2)}{a^2}\frac{\partial^2}{\partial \theta^2} - \frac{\gamma}{{c_L}^2}\frac{\partial^2}{\partial t^2}, \quad L_{12} = \frac{q_2}{a}\frac{\partial^2}{\partial x \partial \theta},$$

$$L_{13} = \frac{\upsilon}{a}\frac{\partial}{\partial x} - \beta^2 a\frac{\partial^3}{\partial x^3} + \beta^2\frac{q_1}{a}\frac{\partial^3}{\partial x \partial \theta^2}$$

$$L_{21} = \frac{q_2}{a}\frac{\partial^2}{\partial x \partial \theta}, \quad L_{22} = d_1\frac{\partial^2}{\partial \theta^2} + d_2\frac{\partial^2}{\partial x^2} - \frac{\gamma}{{c_L}^2}\frac{\partial^2}{\partial t^2},$$

$$L_{23} = d_3\frac{\partial}{\partial \theta} + d_4\frac{\partial^3}{\partial \theta^3} - d_5\frac{\partial^3}{\partial x^2 \partial \theta}$$

$$L_{31} = \frac{\upsilon}{a}\frac{\partial}{\partial x} - \beta^2 a\frac{\partial^3}{\partial x^3} + \frac{\beta^2}{a}q_1\frac{\partial^3}{\partial x \partial \theta^2},$$

$$L_{32} = d_3\frac{\partial}{\partial \theta} + d_4\frac{\partial^3}{\partial \theta^3} - d_5\frac{\partial^3}{\partial x^2 \partial \theta}$$

$$L_{33} = d_6 + d_7\frac{\partial^2}{\partial \theta^2} - \beta^2\left(d_8 + d_9\frac{\partial^2}{\partial \theta^2} + a^2\frac{\partial^4}{\partial x^4}\right.$$

$$\left. + d_{10}\frac{\partial^4}{\partial x^2 \partial \theta^2} + d_{11}\frac{\partial^4}{\partial \theta^4}\right) + \frac{\gamma}{{c_L}^2}\frac{\partial^2}{\partial t^2}$$

where

$$\beta = \frac{h}{\sqrt{12}a}, \qquad q_1 = \frac{1-\upsilon}{2}, \qquad q_2 = \frac{1+\upsilon}{2},$$

$$\gamma = \left(1 + \frac{A}{bh} + \frac{m_{eq}}{\rho h}\right)$$

$$d_1 = \frac{1+\mu}{a^2}, \qquad d_2 = q_1\left(1+3\beta^2\right), \qquad d_3 = \frac{1+\mu+\chi+\beta^2\eta}{a^2}$$

$$d_4 = \frac{\chi+\beta^2\eta}{a^2}, \qquad d_5 = \beta^2\frac{3-\upsilon}{2}, \qquad d_6 = \frac{1+\mu+2\chi}{a^2},$$

$$d_7 = \frac{2\chi}{a^2} \qquad d_8 = \frac{1+3\eta}{a^2}, \qquad d_9 = \frac{2+4\eta}{a^2}, \qquad d_{10} = 2+\eta_t,$$

$$d_{11} = \frac{1+\eta}{a^2}, \qquad \mu = \frac{(1-\upsilon^2)EA}{Ebh}$$

$$\chi = \frac{(1-\upsilon^2)EAz_e}{Ebha}, \qquad \eta = \frac{EI}{bD}, \qquad \eta_t = \frac{GJ}{bD},$$

$$D = \frac{Eh^3}{12(1-\upsilon^2)}.$$

β is the thickness parameter. The ring stiffeners have cross sectional area A, b is the stiffener spacing and z_e is the distance between the shell mid-surface and the centroid of a ring. G is the shear modulus, I is the area moment of inertia of the stiffener about its centroid and J is the polar moment of inertia of the cross sectional area. m_{eq} is the equivalent distributed mass on the cylindrical shell to take into account the onboard equipment and the ballast tanks.